Du, V. A., Jurca, T., Whittell, G. R., & Manners, I. (2016). Aluminum Borate Nanowires from the Pyrolysis of Polyaminoborane Precursors. Dalton Transactions, 45(3), 1055-1062. DOI: 10.1039/C5DT03324A

Dalton Transactions

PAPER

View Article Online
View Journal | View Issue

Cite this: *Dalton Trans.*, 2016, **45**, 1055

Aluminum borate nanowires from the pyrolysis of polyaminoborane precursors†

Van An Du,‡ Titel Jurca,‡ George R. Whittell* and Ian Manners*

Received 27th August 2015,
Accepted 11th November 2015

DOI: 10.1039/c5dt03324a

www.rsc.org/dalton

Polyaminoboranes $[N(R)H\text{-}BH_2]_n$ (**1**: R = H, **2**: R = Me) were pyrolyzed on a range of substrates: silicon, metal foils (stainless steel, nickel, and rhodium), and sapphire wafers, as well as on Al_2O_3 and AlN powders. The pyrolysis of **2** on a Si-wafer resulted in porous nanostructures containing hexagonal-boron nitride (h-BN). In the case of **1** or $H_3N{\cdot}BH_3$ as precursor, using rhodium foil as substrate afforded amorphous B and N-containing nanostructures, and polydisperse spherical nanoparticles, respectively. Switching the substrate to sapphire wafers, as well as to Al_2O_3 or AlN powders, resulted in formation of crystalline Al_5BO_9 nanostructures (nanowires, nanotubes, and nanoribbons). For sapphire wafers, the size of the resulting nanowires was influenced by modifying the surface defect density.

Introduction

Over the past decade, the intense interest in amine-boranes as hydrogen storage materials[1] has led to a broad exploration of other aspects of amine-borane chemistry. This has fostered new uses for amine-boranes as reducing and hydrogen transfer agents,[2] and recently as substrates in the transition-metal catalyzed synthesis of inorganic boron-containing polymers that may possess novel materials properties.[3]

Boron nitride (BN) in its various forms (*e.g.* nanotubes, nanowires, atomically thin films) features high thermal stability, high mechanical strength, resistance to both corrosion and oxidation, as well as useful electrical properties, such as high resistance and low dielectric constant.[4] Since the discovery of graphene in 2004,[5] hexagonal boron nitride (h-BN), the BN-based structural equivalent of graphite, has garnered much attention. Whereas single layers of graphite (graphene) have zero band gap, h-BN is a wide-band gap semiconductor (~6 eV) with promising applications in UV lasing and as a dielectric.[6] Hexagonal boron nitride materials are typically prepared by vapour deposition, condensed-phase pyrolysis of molecular reagents, or preceramic polymer routes.[6c,7]

Due to their high gravimetric content of boron and nitrogen (*ca.* 80% for $H_3N{\cdot}BH_3$), which is already intimately pre-mixed in the required 1 : 1 ratio, amine-boranes are an attractive, potential single-source precursor to BN materials.[7f,g] Polyborazylenes,[7i,j] which have been used as precursors to BN-based ceramics, and other boron–nitrogen containing polymers, such as polyaminoboranes,[3] have similar attributes, along with the advantage of easy scale up and facile macromolecular processing.[7f–k] Herein, we report the pyrolysis of polyaminoboranes $[N(R)H\text{-}BH_2]_n$ (**1**: R = H, **2**: R = Me) on a range of substrates: silicon, metal foils (stainless steel, nickel, and rhodium), and sapphire wafers, as well as Al_2O_3 and AlN powders. The pyrolysis of polyaminoboranes on Si-wafers and rhodium foil afforded BN-containing nanostructures. However, sapphire wafers, as well as Al_2O_3 and AlN powders resulted in the formation of aluminum borate nanomaterials. As discussed below, the latter material is of interest for a range of potential applications as a high performance ceramic.

Experimental

General procedures

Reactions were performed under nitrogen or argon using dry solvents. All chemicals were purchased from Aldrich and used as received unless otherwise noted. Silicon and sapphire wafers were purchased from Wafer World, and Roditi International, respectively. Ammonia borane was obtained from Aldrich and purified by sublimation (T = 40 °C, $p = 10^{-3}$ mbar) prior to use. THF was dried using a Grubb's solvent purification system.[8] Dehydropolymerization catalyst Ir-H_2POCOP (POCOP = 2,6-bis(di-tertbutylphosphinito)-benzene) was synthesized according to the literature.[9] Polyaminoboranes (**1** and **2**) were synthesized according to the iridium-catalyzed method as previously described in the literature (Scheme 1).[3b,c]

Polymers were precipitated at −78 °C in *n*-pentane. Isolated polyaminoborane **2** was found to have M_n = 54 000 g mol^{-1},

School of Chemistry, University of Bristol, Bristol, BS8 1TS, UK.
E-mail: ian.manners@bristol.ac.uk, g.whittell@bristol.ac.uk

†Electronic supplementary information (ESI) available. See DOI: 10.1039/c5dt03324a

‡These authors contributed equally to this work.

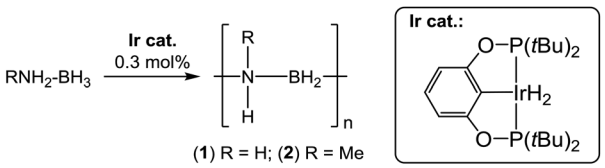

Scheme 1 Synthesis of polyaminoboranes **1** and **2**.

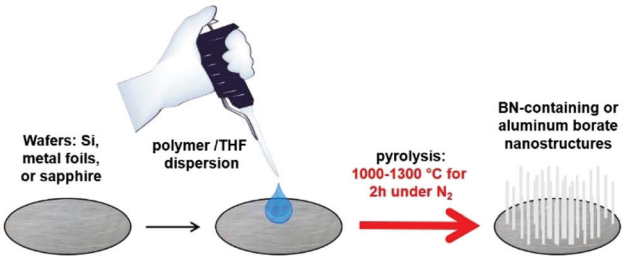

Fig. 1 Preparation and growth of nanostructures from BN-containing precursors on silicon, metal foil or sapphire wafers.

and PDI = 1.32 by GPC. Polymers or $H_3N{\cdot}BH_3$ were dropcast from 2 mg mL^{-1} solutions/dispersions in THF onto the respective substrates: silicon, metal foil {stainless steel (composition Fe : Cr : Ni; 70 : 19 : 11 wt%), nickel, and rhodium}, and sapphire wafers. Additional experiments were conducted with 1 : 1 by mass mixtures of **1** with Al_2O_3 or AlN powders. Pyrolysis experiments were carried out in a horizontal carbolite tube furnace (type 3508), within a 74 mm (outer diameter) by 1250 mm quartz tube, under a nitrogen flow (50 mL min^{-1}) with a heating rate of 10 °C min^{-1} to 1000–1300 °C. The time required to heat to these temperatures is included in the pyrolysis time given (Fig. 1).

Equipment

Conventional calibration gel permeation chromatography (GPC-CC) measurements were carried out at 35 °C at a flow rate of 1.0 mL min^{-1} in nBu$_4$NBr/THF (0.1 wt% nBu$_4$NBr) on a Viscotek GPCmax equipped with both a UV-Vis detector operating at 450 nm and differential refractometer. The column was calibrated with polystyrene standards. Samples were dissolved in THF (1.00 mg mL^{-1} unless otherwise stated) and filtered with Ministart SRP 15 filters (pore size 0.45 μm) prior to analysis. For powder X-ray diffraction measurements, the samples were placed onto a silicon wafer and data were collected with Cu-Kα radiation (λ = 1.5418 Å) on a Bruker D8 Advance powder diffractometer fitted with a 2 mm fixed divergence slit. Data were collected between 10–50 or 10–100 degrees 2θ in θ/2θ mode with a step width of 0.5°. Thermogravimetric analysis (TGA) was performed on a TA Instruments Q500 thermogravimetric analyzer from 20 to 1000 °C at a scan rate of 10 °C min^{-1} under a flow of N_2.

The samples for electron microscopy were prepared by drop casting one drop of suspension of the sample in MeOH onto a carbon coated copper grid which was placed on a piece of filter paper to remove excess solvent. Bright field transmission electron microscopy (TEM) micrographs were obtained on a JEOL 1200 Mk2 TEM microscope operating at 120 kV and equipped with an SIS MegaViewIII digital camera. High resolution images were recorded with a Gatan ORIUS Digital Camera in a JEOL Hi Resolution TEM 2011. Energy-dispersive X-ray (EDX) spectra (spot size of 35 nm) were obtained with an Oxford Instruments ISIS 310 system equipped with a ATW Si (Li) X-ray detector. Scanning electron microscope (SEM) measurements were carried out with a JEOL SEM 5600 LV and a JEOL Field Emission Gun SEM 6330. The samples were mounted onto a sample stub using double sided carbon tape and coated with Ag (15–20 nm). Wavelength-Dispersive X-Ray Spectroscopy (WDS) experiments were carried out with a JEOL JXA8530F Hyperprobe Electron Probe Microanalyser (EPMA) with 5 wavelength dispersive spectrometers and a SDD-EDS (silicon drift detector energy dispersive spectrometer) detector. Operating conditions: (for polymer pyrolyzed on AlN) 5 kV, 100 nA and 10 μm beam, (for polymer pyrolyzed on Al_2O_3) 5 kV, 150 nA and 1 μm beam, and (remaining samples) 5 kV, 150 nA, and 10 μm beam.

Results

Thermogravimetric analysis of polyaminoboranes 1 and 2

The TGA thermogram of **1** indicated thermal stability up to 170 °C, during which a mass loss of only 2% was observed. Past this temperature, sharp decomposition ensued, which was complete by 210 °C and accounted for a 60% mass loss. Continued heating to 1000 °C resulted in minimal further decomposition, giving an ultimate ceramic yield of 34% (Fig. S1a†). In a similar manner, the TGA thermogram of **2** indicated stability to mass loss up to 100 °C, after which an 8% mass loss ensued up to 140 °C, followed by sharp decomposition by 150 °C, resulting in 80% total mass loss. Continued heating to 1000 °C gave an ultimate ceramic yield of 16% (Fig. S1b†). Based on these results, we performed pyrolysis of **1** and **2** on a preparative scale with a variety of substrates under similar conditions (1000 °C under flow of N_2).

Pyrolysis of polyaminoboranes 1 and 2 on silicon wafers

Initial work focused on the attempted formation of BN-containing nanostructures by pyrolysis of polyaminoboranes **1** and **2** on silicon wafers. These surfaces are relatively unreactive, thus providing an opportunity to study the high-temperature chemistry of **1** and **2** independent of substrate effects. Attempted pyrolysis (2 h, at 1000 °C under flow of N_2) of **1** was unsuccessful, leading to depolymerisation and resulting in only trace amounts of material on the wafer post-pyrolysis. Analogous treatment of **2**, however, resulted in the formation of a material that exhibited micron-scale porosity due to the presence of nanoscale fibres (Fig. S2†).[10] XRD revealed a high intensity reflection at 2θ = 27.8° and one of lower intensity at 2θ = 40.9° (Fig. S3†) which could be indexed to the (0 0 2) and

(1 0 0) lattice planes of h-BN, respectively (ICSD: 168892). The presence of B and N (in addition to C and O) was suggested by SEM-EDX (Fig. S4†).

The use of a Si-substrate also appeared to exert an influence on the ceramic yield. The samples obtained from the pyrolysis of **2** in a ceramic combustion crucible displayed a ceramic yield of 8%, while those obtained on a Si-wafer showed a nearly ten-fold increase to 77%. We postulate that this may be due to an anchoring effect facilitated by reaction between the B–H bonds of the polymer and the –OH groups on the surface of the Si-wafer.

Pyrolysis of polyaminoboranes 1 and 2 on metal foils

We then turned our attention to the pyrolysis of polyaminoboranes **1** and **2** on metal foils; namely stainless-steel (composition Fe : Cr : Ni; 70 : 19 : 11 wt%) and nickel (99%). The precedents established for the heterogeneous catalytic dehydrocoupling of amine-boranes by both iron, and nickel-based catalysts make these metal foils intriguing as both substrates and catalysts for the formation of extended BN nanostructures from amine-borane based precursors.[11] Moreover, there are multiple examples of BN nanostructures being grown from both stainless steel and nickel substrates utilizing alternative precursors.[12] However, in the case of **1** and **2**, neither substrate proved successful. Pyrolysis (2 h, at 1000 °C under flow of N_2) of **1** on stainless-steel foil resulted in the formation of micron-sized needles that appear to grow from the surface (Fig. S5†). Pyrolysis of **1** on nickel foil, however, afforded platelets that were polydisperse in size but predominately >1 μm in the shortest observed dimension (Fig. S6†). In neither case were B- and N-containing materials detected by EDX (see Fig. S7 and S8†). In both instances, the structures were most probably comprised of metal oxides.[13]

There is also extensive precedence for heterogeneous catalytic dehydrocoupling of amine-boranes by rhodium-based catalysts.[3e,14] This prompted a similar study into the applicability of Rh foil as both a substrate and catalyst for the formation of extended BN nanostructures utilizing amine-boranes as precursors. Pyrolysis (2 h, at 1000 °C under flow of N_2) of both **1** and **2** on 0.025 mm Rh foil resulted in the formation of nanostructures (Fig. 2a and b for **1**), which were found to contain B and N (in addition to C and O) by SEM-EDX (Fig. S9†). No Bragg reflections were observed by XRD for these samples, which is consistent with an amorphous structure.

Pyrolysis of $H_3N{\cdot}BH_3$, the precursor to **1**, on 0.025 mm Rh foil resulted in the formation of spherical nanoparticles (Fig. 2c and d), which were confirmed to contain B and N by SEM-EDX (Fig. S10†). The particles were polydisperse in size, with diameters ranging from 40–205 nm (Fig. 2c and d). They were, however, difficult to remove from the Rh foil, thus hampering a more thorough study by high-resolution TEM (Fig. 2d). Attempted characterization by XRD and TEM revealed that they are likely amorphous in structure and more polydisperse in size than previously reported examples of spherical BN-containing nanoparticles.[15] Conventional methods for growth of spherical BN-containing nanoparticles rely on more complex aerosol assisted, or chemical vapour deposition (CVD) methodology utilizing multicomponent precursors.[15]

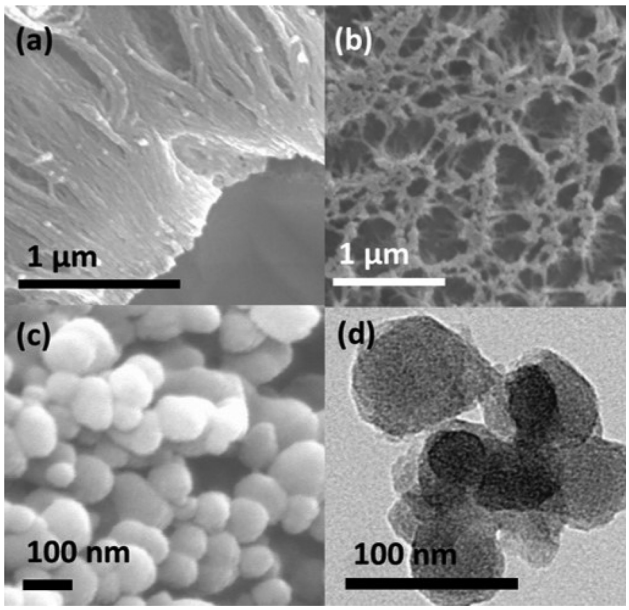

Fig. 2 Electron microscopy images of (a, b, SEM images) amorphous B and N-containing nanostructures grown from pyrolysis (2 h, at 1000 °C under flow of N_2) of polyaminoborane **1** on rhodium foil, and (c, SEM image, d, TEM image) spherical nanoparticles grown from the pyrolysis (2 h, at 1000 °C under flow of N_2) of $H_3N{\cdot}BH_3$ on rhodium foil.

Pyrolysis of polyaminoboranes 1 and 2 on sapphire wafers

As sapphire substrates have previously been utilized for the growth of polycrystalline h-BN *via* metal organic chemical vapour deposition (MO-CVD) of triethylborane and ammonia at 750–1200 °C,[16] we expected sapphire wafers to facilitate the conversion of polyaminoboranes **1** and **2** to h-BN *via* pyrolysis. However, the pyrolysis (2 h, at 1000 °C under flow of N_2) of polyaminoborane **1** on sapphire wafer resulted in the formation of aluminum borate nanowires. The resulting wires grew in high density, and appeared as rough-surfaced rectangular prisms of various lengths and with widths in the range of 100–150 nm (Fig. 3).

In a similar experiment employing a mixture of B and B_2O_3 as the feedstock, these species were comprised predominately of Al_5BO_9, but with a small component of $Al_4B_2O_9$, as determined by XRD.[17a] Unfortunately, the similarity of the two aluminium borate structures, and the relatively low quality of our XRD data (Fig. 4) precludes such a distinction from being made. Having performed the pyrolysis under similar conditions to that with B/B_2O_3, however, and employing a relatively boron-poor precursor, it would appear most likely that we too have formed the aluminium-rich phase predominantly, namely Al_5BO_9. Thus, the four reflections at 2θ = 16.7, 17.0, 26.7 and 33.7° were indexed to the (0 2 1), (1 1 0), (1 3 1) and (1 3 2) planes of the orthorhombic phase of Al_5BO_9 (ICSD: 039013). It is noteworthy, however, that the intense reflection

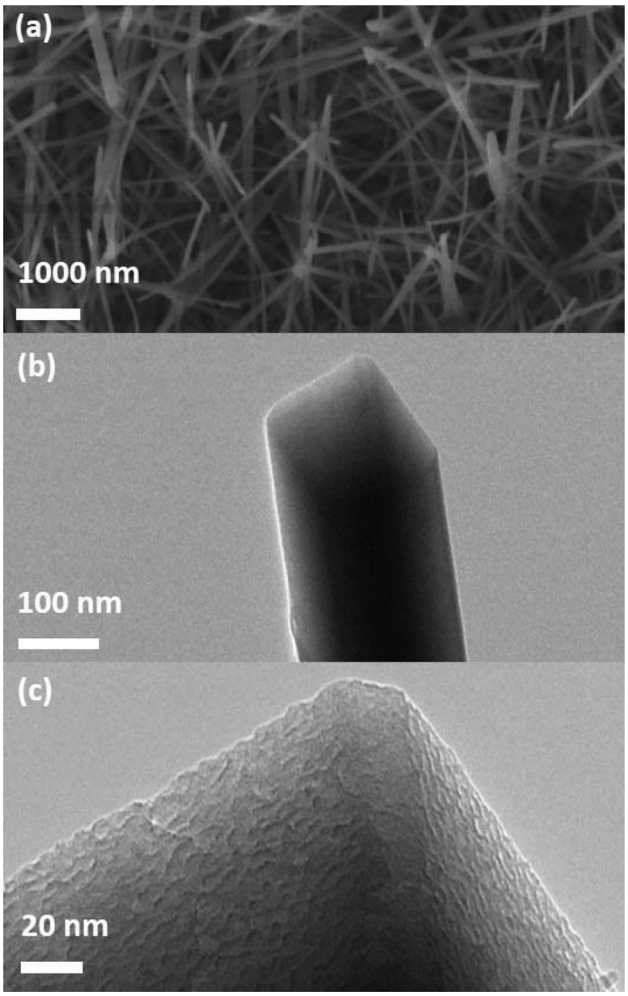

Fig. 3 Electron microscopy images of Al_5BO_9 nanowires grown by pyrolysis (2 h, at 1000 °C under flow of N_2) of polyaminoborane **1** on sapphire with defects; (a) SEM image, (b) and (c) TEM images of a single Al_5BO_9 nanowire.

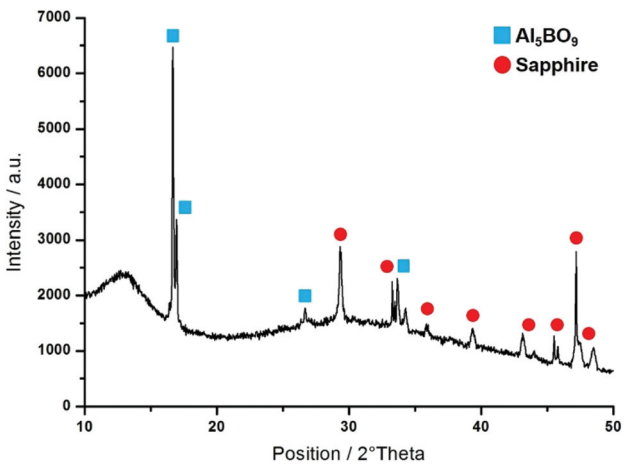

Fig. 4 XRD measurement of Al_5BO_9 nanowires grown by pyrolysis (2 h, at 1000 °C under flow of N_2) of **1** on sapphire with defects.

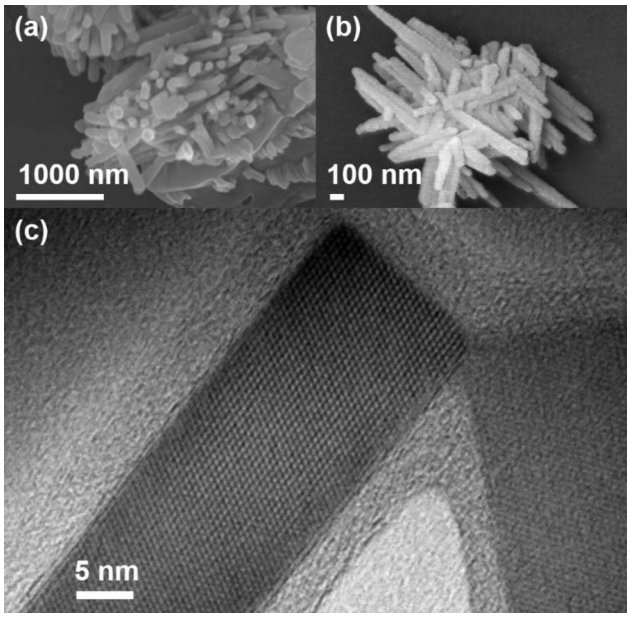

Fig. 5 Electron microscopy images of Al_5BO_9 nanowires grown from the pyrolysis (2 h, at 1000 °C under flow of N_2) of a (1 : 1 by mass) mixture of Al_2O_3 powder and polyaminoborane **1**. (a), (b) SEM images, and (c) high resolution TEM image of a single Al_5BO_9 nanowire.

expected at 2θ = 20.4°, arising from the (1 1 1) plane was not observed. We attribute this phenomenon to the orientation of the nanowires with respect to the substrate, and note that this was also the case when B/B_2O_3 feedstock was employed. The presence of Al, B, and O was confirmed by TEM-EDX and WDS measurements (Fig. S11 and S12†). Nucleation and nanowire growth appears to occur along defects,[17] and thus optimized conditions included introducing defects on the sapphire wafer by scratching the surface with a diamond-tip knife prior to drop-casting the THF dispersion of **1**.

Pyrolysis (2 h, at 1000 °C under flow of N_2) of a (1 : 1 by mass) mixture of Al_2O_3 powder and polyaminoborane **1** also resulted in the formation of clusters of aluminum borate nanowires (Fig. 5). High resolution TEM revealed nanowires with diameters as small as 30 nm (Fig. 5c). In this instance, the XRD diffraction pattern (Fig. S13†) was in agreement with the standard powder diffraction pattern of orthorhombic Al_5BO_9 (ICSD: 039013), including the observation of the (1 1 1) reflection that was absent for the measurement performed on sapphire. Moreover, the lattice fringes observed in Fig. 5c and S14† featured a *d*-spacing of 0.44 nm, and were indexed to the (1 1 1) plane of Al_5BO_9 (ICSD: 039013). It should be noted, however, that as the presence of $Al_4B_2O_9$ cannot be definitely excluded by the XRD pattern of the bulk sample, the alternative assignment of the *d*-spacing to the (1 1 1) plane of $Al_4B_2O_9$ (ICSD: 071113) cannot either. The presence of Al, B, and O was confirmed by SEM-EDX, and WDS measurements (Fig. S15 and S16†). The ~5 nm coating observed in Fig. 5c is probably a partially ordered layer of carbon covering the crystalline aluminum borate core; measurement by TEM-EDX revealed an

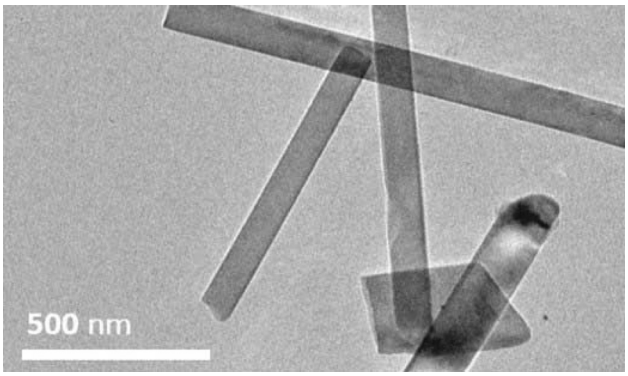

Fig. 6 TEM image of Al_5BO_9 nanoribbons grown from the pyrolysis (2 h, at 1000 °C under flow of N_2) of a (1 : 1 by mass) mixture of AlN powder and polyaminoborane **1**.

appreciable carbon content (Fig. S17†). Additionally, the presence of a low intensity peak at $2\theta = 26.5°$, as observed in the XRD diffraction pattern (Fig. S13†) may be indexed to the (0 0 2) plane of graphite (ICSD: 53781), further supporting our tentative assertion.

Similarly, pyrolysis (2 h, at 1000 °C under flow of N_2) of a (1 : 1 by mass) mixture of AlN powder and **1** was attempted. AlN buffer layers had previously been utilized by Chubarov *et al.* for the growth of rhombohedral-BN.[18] However in our case, inclusion of AlN resulted in the formation of clusters of rectangular aluminum borate nanoribbons featuring widths in the 100–200 nm range, as observed by TEM (Fig. 6). As with the reaction on Al_2O_3, XRD measurements (Fig. S18†) revealed the presence of what is most likely Al_5BO_9 (ICSD: 039013) on account of the boron-content in **1** relative to B/B_2O_3 and the product mixture observed when the latter was used as the feedstock.[17a] The presence of Al, B, and O was confirmed by SEM-EDX and WDS measurements (Fig. S19 and S20†).

Finally, pyrolysis of polyaminoborane **2** on annealed sapphire wafer (2 h, at 1300 °C, under flow of N_2, no induced defects) also resulted in the formation of aluminum borate nanowires and, in addition, nanotubes (Fig. S21†). Unlike previous trials utilizing **1** on defect-laden sapphire surface, the use of a smooth sapphire surface resulted in rectangular nanowires, which were significantly larger in size (some greater than 1000 nm in diameter) and appeared, in some cases, to be hollow (Fig. S21†). The XRD diffraction pattern (Fig. S22†) was again consistent with the orthorhombic phase of Al_5BO_9 (ICSD: 039013). The presence of Al, B, and O was similarly confirmed by SEM-EDX analysis (Fig. S23†).

Discussion

Bulk aluminum borates are attractive materials owing to their many useful properties, such as high strength, chemical inertness, high temperature stability, which includes resistance to oxidation at high temperatures and a low coefficient of thermal expansion.[19] Moreover, one-dimensional nanostructures, such as nanowires, often have intriguing properties that differ from those of bulk materials. These include quantum confinement of electrons by the potential wells of nanometer-sized structures, which may allow control of electrical, optical, magnetic, and thermoelectric properties of solid-state functional materials.[20] This has led to potential applications of aluminum borate nanostructures in ceramic composites, metal matrix composites, tribology, and as building blocks in optoelectronics.[21]

Surprisingly, polyaminoboranes **1** and **2** have proven to be excellent precursors for the facile fabrication of aluminum borate nanowires (*via* **1**) and in some cases larger nanotubes (*via* **2**) on sapphire substrates. The ability to use a stable, single-source precursor which can be delivered with ease *via* drop-casting on a substrate or mixed with a powder of Al_2O_3 or AlN for the synthesis of aluminium borate nanowires proves advantageous over more conventional techniques. Aluminum borate nanowire synthesis typically requires multiple reagents, catalysts, or more complex chemical vapour deposition (CVD) methodology with subsequent pyrolysis at temperatures ranging from 750–1100 °C.[22] In the instance of sapphire wafer as substrate, the size of the resulting nanowires was influenced by modifying the surface defect density. While pyrolysis of polyaminoboranes on smooth sapphire led to nanowires, and in some cases, nanotubes, with diameters greater than 1000 nm, introducing surface defects produced nanowires with diameters in the 100–150 nm range.

Rümmeli and coworkers have recently reported the synthesis of $Al_4B_2O_9$ and Al_5BO_9 nanowires from the pyrolysis (700–1100 °C) of a mixture of B and B_2O_3 (3 : 4 by mass) on sapphire wafers,[17a] a process reminiscent of our procedure. Samples pyrolyzed on smooth surfaces resulted in slower formation of larger diameter nanowires, whereas samples with defects (induced by incorporation of Fe_3O_4 nanoparticles) resulted in the facile formation of smaller diameter nanowires. The growth mechanism was attributed to diffusion of boron into the sapphire wafer, a process which occurs more readily at surface defects, followed by initial surface corrugation, and ultimately nanowire formation, which occurs as a measure to alleviate the stress build up from the resulting thermal expansion mismatch as aluminum oxide becomes aluminum borate.[17a] Thus, we propose a similar growth mechanism, whereby B–N based precursor (polyaminoborane **1** or **2**) either decomposes, leading to diffusion of B into the alumina surface, or diffuses directly into the alumina surface, where N is released, and growth of aluminum borate nanowires begins. This is consistent with defect-laden sapphire resulting in smaller diameter nanowires, and smooth surface sapphire resulting in a slower formation of larger diameter nanowires; this is also consistent with previously reported observations.[17a]

The fabrication of $Al_4B_2O_9$ nanowhiskers on the surface of aluminum powder with boric acid as boron source has recently been described by Shi and coworkers.[22] It was proposed that during pyrolysis (600–800 °C), boric acid decomposed to B_2O_3

and the Al_2O_3 layer formed on the aluminum powder dissolved into the liquid B_2O_3 (mp 450 °C), initiating nanostructure growth. Overall, the formation of Al_5BO_9 nanowhiskers was described as a solution–liquid–solid (SLS) growth process. A similar process may operate for the Al_5BO_9 nanowire and nanoribbon growth processes described herein for mixtures of polyaminoborane **1** with Al_2O_3 or AlN powders. High temperature decomposition of **1**, in contact with atmospheric O_2 may lead to the generation of B_2O_3, which can interact with Al_2O_3, either already present, or generated from the high temperature reaction of AlN with atmospheric O_2. Alternatively, the growth process may proceed in a similar manner to that described for the pyrolysis of polyaminoboranes on sapphire wafer (*vide supra*).

Conclusions

In the case of Si-wafer as substrate, the pyrolysis of **2** resulted in amorphous nanostructures which feature a component of h-BN. The use of rhodium foil as substrate afforded amorphous B and N-containing nanostructures from the pyrolysis of **1** and **2**, and polydisperse, amorphous B and N-containing spherical nanoparticles from $H_3N{\cdot}BH_3$. Switching the substrate to sapphire wafers, as well as Al_2O_3 and AlN powders, resulted in the unexpected production of crystalline aluminum borate nanowires, most likely Al_5BO_9. In the instance of sapphire wafer substrates, the diameters of the resulting nanowires were dependent on the surface defect density. In the case of smooth surfaces, larger nanowires were produced, whereas defect-laden surfaces facilitated the formation of significantly smaller nanowires. The ability to use polyaminoboranes **1** and **2** as stable precursors to aluminum borate nanowires, which can be delivered with ease *via* drop-casting on a substrate, or mixing with a powder of Al_2O_3 or AlN appears to be potentially advantageous over conventional, more complex approaches (*e.g.* CVD). Optimisation and further development of this process is currently under investigation. We are also investigating polyaminoboranes that undergo thermally-induced crosslinking in order to access BN-containing ceramics in higher yield.

Acknowledgements

V. A. D. thanks the Deutsche Forschungsgemeinschaft (DFG) for a Postdoctoral Fellowship. T. J. thanks the EU for a Marie Curie Postdoctoral Fellowship and EPSRC for support. I. M. also thanks the EPSRC for support. The authors thank the Electron Microscopy Unit (School of Chemistry, University of Bristol) for support with TEM measurements, and Dr B. Buse (School of Earth Sciences, University of Bristol) for support with WDS measurements. J. Gwyther (University of Bristol) is thanked for helpful discussions.

References

1 (*a*) A. Staubitz, A. P. M. Robertson and I. Manners, *Chem. Rev.*, 2010, **110**, 4079–4124; (*b*) A. Karkamkar, C. Aardahl and T. Autrey, *Mater. Matters*, 2007, **2**, 6–10; available at http://www.sigmaaldrich.com/materials-science/learning-center/material-matters.html (*c*) B. Peng and J. Chen, *Energy Environ. Sci.*, 2008, **1**, 479–483; (*d*) F. H. Stephens, V. Pons and R. T. Baker, *Dalton Trans.*, 2007, 2613–2626; (*e*) N. C. Smythe and J. C. Gordon, *Eur. J. Inorg. Chem.*, 2010, 509–521; (*f*) O. T. Summerscales and J. C. Gordon, *Dalton Trans.*, 2013, **42**, 10075–10084; (*g*) M. E. Bluhm, M. G. Bradley, R. Butterick III, U. Kusari and L. G. Sneddon, *J. Am. Chem. Soc.*, 2006, **128**, 7748–7749; (*h*) D. W. Himmelberger, C. W. Yoon, M. E. Bluhm, P. J. Carroll and L. G. Sneddon, *J. Am. Chem. Soc.*, 2009, **131**, 14101–14110.

2 (*a*) A. Staubitz, A. P. M. Robertson, M. E. Sloan and I. Manners, *Chem. Rev.*, 2010, **110**, 4023–4078; (*b*) E. M. Leitao, N. E. Stubbs, A. P. M. Robertson, H. Helten, R. J. Cox, G. C. Lloyd-Jones and I. Manners, *J. Am. Chem. Soc.*, 2012, **134**, 16805–16816; (*c*) M. E. Sloan, A. Staubitz, K. Lee and I. Manners, *Eur. J. Org. Chem.*, 2011, 672–675; (*d*) X. Yang, L. Zhao, T. Fox, Z.-X. Wang and H. Berke, *Angew. Chem., Int. Ed.*, 2010, **49**, 2058–2062; (*e*) X. Yang, T. Fox and H. Berke, *Chem. Commun.*, 2011, **47**, 2053–2055; (*f*) C. C. Chong, H. Hirao and R. Kinjo, *Angew. Chem., Int. Ed.*, 2014, **53**, 3342–3346.

3 (*a*) E. M. Leitao, T. Jurca and I. Manners, *Nat. Chem.*, 2013, **5**, 817–829; (*b*) A. Staubitz, A. Presa Soto and I. Manners, *Angew. Chem., Int. Ed.*, 2008, **47**, 6212–6215; (*c*) A. Staubitz, M. E. Sloan, A. P. M. Robertson, A. Friedrich, S. Schneider, P. J. Gates, J. Schmedt auf der Günne and I. Manners, *J. Am. Chem. Soc.*, 2010, **132**, 13332–13345; (*d*) A. N. Marziale, A. Friedrich, I. Klopsch, M. Drees, V. R. Celinski, J. Schmedt auf der Günne and S. Schneider, *J. Am. Chem. Soc.*, 2013, **135**, 13342–13355; (*e*) H. C. Johnson, E. M. Leitao, G. R. Whittell, I. Manners, G. C. Lloyd-Jones and A. S. Weller, *J. Am. Chem. Soc.*, 2014, **136**, 9078–9093.

4 (*a*) N. G. Chopra, R. J. Luyken, K. Cherrey, V. H. Crespi, M. L. Cohen, S. G. Louie and A. Zettl, *Science*, 1995, **269**, 966–967; (*b*) K. F. Huo, Z. Hu, F. Chen, J. J. Fu, Y. Chen, B. H. Liu, J. Ding, Z. L. Dong and T. White, *Appl. Phys. Lett.*, 2002, **80**, 3611–3613; (*c*) Y. Kubota, K. Watanabe, O. Tsuda and T. Taniguchi, *Science*, 2007, **317**, 932–934; (*d*) M. Corso, W. Auwärter, M. Muntwiler, A. Tamai, T. Greber and J. Osterwalder, *Science*, 2004, **303**, 217–220.

5 K. S. Novoselov, A. K. Geim, S. V. Morozov, D. Jiang, Y. Zhang, S. V. Dubonos, I. V. Grigorieva and A. A. Firsov, *Science*, 2004, **306**, 666–669.

6 (*a*) G. R. Whittell and I. Manners, *Angew. Chem., Int. Ed.*, 2011, **50**, 10288–10289; (*b*) D. Golberg, Y. Bando, Y. Huang, T. Terao, M. Mitome, C. Tang and C. Zhi, *ACS Nano*, 2010, **4**, 2979–2993; (*c*) K. K. Kim, A. Hsu, X. Jia, S. M. Kim, Y. Shi, M. Dresselhaus, T. Palacios and J. Kong, *ACS Nano*, 2012, **6**, 8583–8590.

7 Selected examples: (*a*) R. T. Paine and C. K. Narula, *Chem. Rev.*, 1990, **90**, 73–91; (*b*) A. Ismach, H. Chou, D. A. Ferrer, Y. Wu, S. McDonnell, H. C. Floresca, A. Covacevich, C. Pope, R. Piner, M. J. Kim, R. M. Wallace, L. Colombo and R. S. Ruoff, *ACS Nano*, 2012, **6**, 6378–6385; (*c*) S. Schlienger, J. Alauzun, F. Michaux, L. Vidal, J. Parmentier, C. Gervais, F. Babonneau, S. Bernard, P. Miele and J. B. Parra, *Chem. Mater.*, 2012, **24**, 88–96; (*d*) J. Li, S. Bernard, V. Salles, C. Gervais and P. Miele, *Chem. Mater.*, 2010, **22**, 2010–2019; (*e*) A. Nag, K. Raidongia, K. P. S. S. Hembram, R. Datta, U. V. Waghmare and C. N. R. Rao, *ACS Nano*, 2010, **4**, 1539–1544; (*f*) S. K. Kim, H. Cho, M. J. Kim, H. J. Lee, J. Park, Y.-B. Lee, H. C. Kim, C. W. Yoon, S. W. Nam and S. O. Kang, *J. Mater. Chem. A*, 2013, **1**, 1976–1981; (*g*) D.-P. Kim, K.-T. Moon, J.-G. Kho, J. Economy, C. Gervais and F. Babonneau, *Polym. Adv. Technol.*, 1999, **10**, 702–712; (*h*) L. G. Sneddon, M. G. L. Mirabelli, A. T. Lynch, P. J. Fazen, K. Su and J. S. Beck, *Pure Appl. Chem.*, 1991, **63**, 407–410; (*i*) P. J. Fazen, E. E. Remsen, J. S. Beck, P. J. Carroll, A. R. McGhie and L. G. Sneddon, *Chem. Mater.*, 1995, **7**, 1942–1956; (*j*) T. Wideman, P. J. Fazen, K. Su, E. E. Remsen, G. A. Zank and L. G. Sneddon, *Appl. Organomet. Chem.*, 1998, **12**, 681–693; (*k*) S. Bernard and P. Miele, *Materials*, 2014, **7**, 7436–7459.

8 A. B. Pangborn, M. A. Giardello, R. H. Grubbs, R. K. Rosen and F. J. Timmers, *Organometallics*, 1996, **15**, 1518–1520.

9 I. Göttker-Schnetmann, P. S. White and M. Brookhart, *Organometallics*, 2004, **23**, 1766–1776.

10 Due to the poor solubility of **1** in THF, this material was cast as a dispersion. This caused an uneven distribution of **1**, and as a result, a higher surface area and less substrate contact, which probably explains the negligible ceramic yield. Conversely, polyaminoborane **2** displayed excellent solubility in THF, and could be dropcast as a coherent thin film.

11 For iron-catalysed dehydrocoupling see: (*a*) J. R. Vance, A. P. M. Robertson, K. Lee and I. Manners, *Chem. – Eur. J.*, 2011, **17**, 4099–4103; (*b*) J. R. Vance, A. Schäfer, A. P. M. Robertson, K. Lee, J. Turner, G. R. Whittell and I. Manners, *J. Am. Chem. Soc.*, 2014, **136**, 3048–3064; (*c*) R. T. Baker, J. C. Gordon, C. W. Hamilton, N. J. Henson, P.-H. Lin, S. Maguire, M. Murugesu, B. L. Scott and N. C. Smythe, *J. Am. Chem. Soc.*, 2012, **134**, 5598–5609; (*d*) C. Lichtenberg, L. Viciu, M. Adelhardt, J. Sutter, K. Meyer, B. de Bruin and H. Grützmacher, *Angew. Chem., Int. Ed.*, 2015, **54**, 5766–5771. For nickel-catalysed dehydrocoupling see: (*e*) A. P. M. Robertson, R. Suter, L. Chabanne, G. R. Whittell and I. Manners, *Inorg. Chem.*, 2011, **50**, 12680–12691; (*f*) R. J. Keaton, J. M. Blacquiere and R. T. Baker, *J. Am. Chem. Soc.*, 2007, **129**, 1844–1845; (*g*) M. Vogt, B. de Bruin, H. Berke, M. Trincado and H. Grützmacher, *Chem. Sci.*, 2011, **2**, 723–727.

12 (*a*) Boron-nitride nanowires grown on stainless-steel substrate from a mixture of B and ZnO at 1100 °C under a mixture of H_2 and N_2: Y. J. Chen, B. Chi, D. C. Mahon and Y. Chen, *Nanotechnology*, 2006, **17**, 2942–2946; (*b*) Heteroepitaxial layers of h-BN grown from triethylboron and ammonia on single crystal Ni(111) substrates at 1020 °C: Y. Kobayashi, T. Nakamura, T. Akasaka, T. Makimoto and N. Matsumoto, *Phys. Status Solidi B*, 2007, **244**, 1789–1792; (*c*) Chemical vapour deposition of BN nanosheets on Cu, and Ni(111) from decaborane under a flow of N_2 and H_2 at 1000 °C: S. Chatterjee, Z. Luo, M. Acerce, D. M. Yates, A. T. C. Johnson and L. G. Sneddon, *Chem. Mater.*, 2011, **23**, 4414–4416; (*d*) Boron-nitride nanotubes synthesized with the aid of floating nickel catalyst *via* catalytic chemical vapour deposition (CCVD) of either borazine ($B_3N_3H_6$) or decaborane at 1200–1300 °C: S. Chatterjee, M. J. Kim, D. N. Zakharov, S. M. Kim, E. A. Stach, B. Maruyama and L. G. Sneddon, *Chem. Mater.*, 2012, **24**, 2872–2879; (*e*) Boron-nitride nanotubes grown by CVD method utilizing Ni, NiB, or Ni_2B particles as catalyst at 1000–1100 °C: O. R. Lourie, C. R. Jones, B. M. Bartlett, P. C. Gibbons, R. S. Ruoff and W. E. Buhro, *Chem. Mater.*, 2000, **12**, 1808–1810.

13 The change in morphology is probably due to the onset of respective metal oxide nanoparticle growth at the high pyrolysis temperatures utilized (1000 °C). In addition, the presence of amine-borane materials, may also contribute to the process *via* interactions with the substrate surface, causing defects which seed metal oxide growth. The presence of oxygen was confirmed by SEM-EDX, see Fig. S7 and S8.†

14 (*a*) C. A. Jaska, K. Temple, A. J. Lough and I. Manners, *Chem. Commun.*, 2001, 962–963; (*b*) C. A. Jaska, K. Temple, A. J. Lough and I. Manners, *J. Am. Chem. Soc.*, 2003, **125**, 9424–9434; (*c*) T. M. Douglas, A. B. Chaplin, A. S. Weller, X. Yang and M. B. Hall, *J. Am. Chem. Soc.*, 2009, **131**, 15440–15456; (*d*) L. J. Sewell, G. C. Lloyd-Jones and A. S. Weller, *J. Am. Chem. Soc.*, 2012, **134**, 3598–3610; (*e*) H. C. Johnson and A. S. Weller, *Angew. Chem., Int. Ed.*, 2015, **54**, 10173–10177.

15 (*a*) D. A. Lindquist, T. T. Kodas, D. M. Smith, X. M. Xiu, S. L. Hietala and R. T. Paine, *J. Am. Ceram. Soc.*, 1991, **74**, 3126–3128; (*b*) C. Tang, Y. Bando and D. Golberg, *Chem. Commun.*, 2002, 2826–2827; (*c*) C. Tang, Y. Bando, Y. Huang, C. Zhi and D. Golberg, *Adv. Funct. Mater.*, 2008, **18**, 3653–3661.

16 K. Nakamura, *Electrochem. Soc.*, 1986, **133**, 1120–1123.

17 (*a*) I. Gonzalez-Martinez, A. Bachmatiuk, S. Gorantla, J. Kunstmann, V. Bezugly, T. Gemming, B. Büchner, G. Cuniberti and M. H. Rümmeli, *J. Appl. Phys.*, 2012, **112**, 024308; (*b*) D. Tsivion, M. Schvartzman, R. Popovitz-Biro and E. Joselevich, *ACS Nano*, 2012, **6**, 6433–6445.

18 M. Chubarov, H. Pedersen, H. Högberg, J. Jensen and A. Henry, *Cryst. Growth Des.*, 2012, **12**, 3215–3220.

19 (*a*) K. Suganuma, T. Fujita, N. Suzuki and K. Niihara, *J. Mater. Sci. Lett.*, 1990, **9**, 633–635; (*b*) R. Ma, Y. Bando, T. Sato, C. Tang and F. Xu, *J. Am. Chem. Soc.*, 2002, **124**, 10668–10669; (*c*) H. S. Song, E. M. Elssfah, J. Zhang, J. Lin, J. J. Luo, S. J. Liu, Y. Huang, X. X. Ding, J. M. Gao, S. R. Qi

and C. Tang, *J. Phys. Chem. B*, 2006, **110**, 5966–5969; (*d*) M. Zheng, K. Wu, H. Liang, S. Kamado and Y. Kojima, *Mater. Lett.*, 2002, **57**, 558–564.

20 See: Y. Xia, P. Yang, Y. Sun, Y. Wu, B. Mayers, B. Gates, Y. Yin, F. Kim and H. Yan, *Adv. Mater.*, 2003, **15**, 353–389, and references therein.

21 (*a*) L. M. Peng, S. J. Zhu, Z. Y. Ma, J. Bi, F. G. Wang, H. R. Chen and D. O. Northwood, *Mater. Sci. Eng., A*, 1999, **265**, 63–70; (*b*) Z. S. Hu, Y. G. Shi, L. G. Wang, Y. Peng, G. X. Chen and J. X. Dong, *Lubr. Eng.*, 2001, **57**, 23–27; (*c*) R. Ma, Y. Bando and T. Sato, *Appl. Phys. Lett.*, 2002, **81**, 3467–3469; (*d*) X. Tao, X. Wang and X. Li, *Nano Lett.*, 2007, **7**, 3172–3176; (*e*) E. M. Elssfah, H. S. Song, C. C. Tang, J. Zhang, X. X. Ding and S. R. Qi, *Mater. Chem. Phys.*, 2007, **101**, 499–504; (*f*) R. K. Gupta, A. A. Al-Ghamdi, O. A. Al-Hartomy, F. Al-Hazmi, F. El-Tantawy and F. Yakuphanoglu, *J. Sol-Gel Sci. Technol.*, 2012, **64**, 100–103; (*g*) Y. Li and R. P. H. Chang, *Mater. Chem. Phys.*, 2006, **97**, 23–30; (*h*) J. Wang, G. Ning, X. Yang, Z. Gan, H. Liu and Y. Lin, *Mater. Lett.*, 2008, **62**, 1208–1211; (*i*) S. H. Kenawy, *Int. J. Appl. Ceram. Technol.*, 2011, **8**, 783–792; (*j*) Y. Liu, Q. Li and S. Fan, *Chem. Phys. Lett.*, 2003, **375**, 632–635; (*k*) L. M. Peng, X. K. Li, H. Li, J. H. Wang and M. Gong, *Ceram. Int.*, 2006, **32**, 365–368; (*l*) H.-T. Sun, F. Shimaoka, M. Fujii, N. Nitta, M. Mizuhata, H. Yasuda, S. Deki and S. Hayashi, *Nanotechnology*, 2009, **20**, 035604.

22 Z. Yu, N. Zhao, E. Liu, C. Shi, X. Du and J. Wang, *Powder Technol.*, 2011, **212**, 310–315.